ACS OMEGA

http://pubs.acs.org/journal/acsodf

Article

A Hierarchical Theoretical Study of the Hydrogen Abstraction Reactions of H_2/C_1-C_4 Molecules by the Methyl Peroxy Radical and Implications for Kinetic Modeling

Shenying Xu, Jinhu Liang,* Shutong Cao, Ruining He, Guoliang Yin, and Quan-De Wang*

Cite This: *ACS Omega* 2022, 7, 8675−8685

Read Online

ACCESS | Metrics & More | Article Recommendations | Supporting Information

ABSTRACT: The hydrogen atom abstraction by the methyl peroxy radical (CH_3O_2) is an important reaction class in detailed chemical kinetic modeling of the autoignition properties of hydrocarbon fuels. Systematic theoretical studies are performed on this reaction class for H_2/C_1-C_4 fuels, which is critical in the development of a base model for large fuels. The molecules include hydrogen, alkanes, alkenes, and alkynes with a carbon number from 1 to 4. The B2PLYP-D3/cc-pVTZ level of theory is employed to optimize the geometries of all of the reactants, transition states, and products and also the treatments of hindered rotation for lower frequency modes. Accurate benchmark calculations for abstraction reactions of hydrogen, methane, and ethylene with CH_3O_2 are performed by using the coupled cluster method with explicit inclusion of single and double electron excitations and perturbative inclusion of triple electron excitations (CCSD(T)), the domain-based local pair-natural orbital coupled cluster method (DLPNO-CCSD(T)), and the explicitly correlated CCSD(T)-F12 method with large basis sets. Reaction rate constants are computed via conventional transition state theory with quantum tunneling corrections. The computed rate constants are compared with literature values and those employed in detailed chemical kinetic mechanisms. The calculated rate constants are implemented into the recently developed NUIGMECH1.1 base model for kinetic modeling of ignition properties.

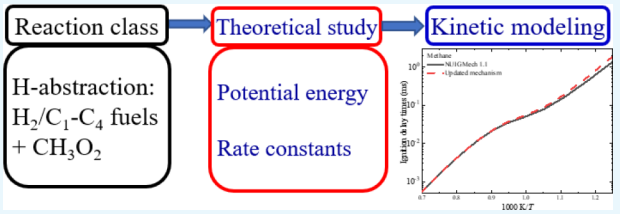

1. INTRODUCTION

The development of detailed chemical kinetic mechanisms to model combustion of hydrocarbon fuels has received significant progress in the past few decades due to its importance in a variety of applications ranging from internal combustion engines to gas turbines.[1−5] With more stringent requirements on pollution emissions, low-temperature oxidation of hydrocarbons has been of great interest to the combustion community.[3,6,7] It has been shown that hydroperoxides play an important role in the low-temperature oxidation of hydrocarbons.[2,8] One possible source of hydroperoxides is the hydrogen abstraction from hydrocarbons by alkyl peroxy radicals.[8,9] In addition, hydrogen atom abstraction by alkyl peroxy radicals is also an important reaction class in the autoignition of fuels, especially at low-to-intermediate temperatures ranging from 600 to 1300 K.[2,8] Although a series of experimental and theoretical studies has been performed on reaction classes related to hydroperoxides and abstraction reactions from hydrocarbons by the hydroperoxyl radical (HO_2),[10−13] abstraction reactions by alkyl peroxy radicals receive less attention. Most of the reaction rate constants used in kinetic models were based on rough estimation or analogy.[14−16] Carstensen et al. initially performed a theoretical study on the abstraction reactions for ethane (C_2H_6) by HO_2, methyl peroxy (CH_3O_2), and ethyl peroxy ($C_2H_5O_2$) radicals by using conventional transition state theory (TST) based on quantum chemical calculations at the CBS-QB3 level of theory.[17] Subsequently, they extended the investigation by considering more alkanes including methane (CH_4), ethane (C_2H_6), propane (C_3H_8), and *n*-butane (C_4H_{10}) abstracted by additional peroxy species (RO_2 with R = H, CH_3, C_2H_5, C_3H_7, C_4H_9, HC═O, and CH_3C═O) by using the same computational methods.[18] It was concluded that the structure of fuels shows a large effect on the rate constants, indicating that systematic studies on this reaction class by including more fuel molecules with enough structural diversity are desired. Hashemi et al. performed high-level theoretical calculations for the abstraction reaction of CH_4 with CH_3O_2, which exhibits high sensitivity during high-pressure oxidation of CH_4.[19] However, no systematic study has been performed to provide accurate rate constants for this reaction class.

In detailed kinetic modeling of all fuels, the reaction rate of H_2/C_1-C_4 base chemistry is among the most sensitive ones controlling the pyrolysis and oxidation processes.[2,5,20,21] The H_2/C_1-C_4 kinetic mechanism is a crucial subgroup of many

Received: November 25, 2021
Accepted: February 18, 2022
Published: March 1, 2022

https://doi.org/10.1021/acsomega.1c06683
ACS Omega 2022, 7, 8675−8685

other hydrocarbons and oxygenated molecules, as well as molecular growth kinetics leading to the formation of soot precursors such as polycyclic aromatic hydrocarbons. Recently, substantial progress was made in identifying the principal global structures of the H_2/C_1-C_4 oxidation mechanism.[5] The NUI Galway group conducted a systematic ignition study on small hydrocarbon fuels, especially focused on low-temperature conditions.[14−16] Kinetic modeling studies indicate that the abstraction reaction for small hydrocarbon fuels by the CH_3O_2 radical is critical in accurate predictions of ignition delay times under low-temperature conditions. Hence, accurate rate constants for this reaction class are desired to refine the H_2/C_1-C_4 base mechanism.

Based on the above considerations, this work aims to compute accurate and consistent rate constants for abstraction reactions of H_2/C_1-C_4 hydrocarbons with the CH_3O_2 radical. The studied H_2/C_1-C_4 hydrocarbons include H_2, alkanes, alkenes, and alkynes with a carbon number ≤4. To provide accurate energy information for rate constant calculations, benchmark reaction barriers and enthalpies for some small reaction systems are performed by using a series of accurate high-level theoretical methods. Rate constants are computed via TST with quantum tunneling corrections. The obtained rate constants are fitted into the modified Arrhenius formula and implemented into the recently developed skeletal NUIGMECH1.1 base model[21] to demonstrate the effect on ignition properties.

This paper has the following structure: first, the computational details to obtain both the reaction barriers and the reaction rate constants are provided in Section 2. Section 3 first provides benchmarking cases to establish the accuracy of the methods employed for rate constants. After this, the computed rate constants are discussed and compared with literature values. The fitted Arrhenius coefficients used for kinetic modeling are presented. Finally, the fitted reaction rate coefficients are implemented into the skeletal NUIGMECH 1.1 mechanisms for kinetic modeling of ignition delay times of typical fuels, and the conclusions are presented in Section 4.

2. COMPUTATIONAL METHODOLOGY

2.1. Geometry Optimization. In order to investigate the structure and reaction site effect on the abstraction reaction class and provide valuable rate constants for small fuel molecules used for kinetic models, all C_1-C_4 hydrocarbons with a carbon number ≤4 and H_2 are considered. To obtain reliable geometries and frequencies, the double-hybrid density functional method (B2PLYP)[22] with dispersion corrections denoted as the B2PLYP-D3 functional[23] together with a cc-pVTZ basis set[24] is employed. Although the B2PLYP-D3 method requires more CPU time compared with widely used B3LYP[25] or M06-2X[26] methods due to the inclusion of the MP2 component, it can approach the accuracy of CCSD(T)/cc-pVTZ geometries and frequencies for most species including transition states (TSs), especially for radical oxidation reactions in combustion and atmosphere chemistry.[27] Zero-point vibrational energies are also obtained at this level based on analytical harmonic frequency calculations. For the treatment of internal rotations, relaxed potential energy scans are also performed as a function of the corresponding dihedral angle with an interval of 10° at this level. The scanned results are fitted to a truncated Fourier series used for rate constant calculations. For the TS structures, intrinsic reaction coordinate (IRC) calculations[28] are carried out to ensure that the saddle points connect the desired reactants and products.

2.2. Single-Point Energy Calculations. To obtain reliable reaction energy barriers and enthalpies, single-point energy calculations are performed with high-level quantum chemistry methods. A series of benchmark calculations is carried out for H_2, CH_4, and C_2H_4 with the CH_3O_2 radical using the coupled cluster method with explicit inclusion of single and double electron excitations and perturbative inclusion of triple electron excitations (CCSD(T)),[29] the domain-based local pair-natural orbital coupled cluster method (DLPNO-CCSD(T)),[30,31] and the explicitly correlated CCSD-(T)-F12 method[32] with large basis sets. Specifically, The CCSD(T) method with cc-pVDZ, cc-pVTZ, and cc-pVQZ basis sets[24,33] extrapolated to the complete basis set (CBS) limit is performed for the three reactions. Two formulas are adopted for the extrapolations, and one is defined as[34] follows:

$$E_{\mathrm{CCSD(T)/CBS}} = E_{\mathrm{CCSD(T)/QZ}} + (E_{\mathrm{CCSD(T)/QZ}} - E_{\mathrm{CCSD(T)/TZ}}) \times \frac{4^4}{5^4 - 4^4} \quad (1)$$

The other formula is based on CCSD(T) with cc-pVDZ and cc-pVTZ calculations in conjunction with corrected energies from the MP2 method with cc-pVDZ, cc-pVTZ, and cc-pVQZ basis sets as[34] follows:

$$\begin{aligned} E_{\mathrm{CCSD(T)-MP2/CBS}} = {} & E_{\mathrm{CCSD(T)/TZ}} \\ & + (E_{\mathrm{CCSD(T)/TZ}} - E_{\mathrm{CCSD(T)/DZ}}) \\ & \times \frac{3^4}{4^4 - 3^4} + E_{\mathrm{MP2/QZ}} \\ & + (E_{\mathrm{MP2/QZ}} - E_{\mathrm{MP2/TZ}}) \times \frac{4^4}{5^4 - 4^4} \\ & - E_{\mathrm{MP2/TZ}} - (E_{\mathrm{MP2/TZ}} - E_{\mathrm{MP2/DZ}}) \\ & \times \frac{3^4}{4^4 - 3^4} \end{aligned} \quad (2)$$

where DZ, TZ, and QZ represent the cc-pVDZ, cc-pVTZ, and cc-pVQZ basis sets, respectively.

The DLPNO-CCSD(T) method has recently been shown to provide an effective procedure for fairly large systems. To demonstrate the accuracy of this method for the studied reaction class, the DLPNO-CCSD(T) method with large basis sets including cc-pVTZ, cc-pVQZ, def2-TZVPP, and def2-QZVPP[35] is also used for the three reactions for benchmark calculations. During DLPNO-CCSD(T) calculations, the set of truncation TightPNO threshold is chosen to keep the accuracy.[36] The explicitly correlated CCSD(T)-F12 method with cc-pVTZ-F12 and cc-pVQZ-F12 basis sets is employed as the benchmark. The T_1 diagnostics during CCSD(T) calculations[37] are used to check the multireference nature of the studied reactions. Generally, a single-reference coupled cluster calculation for closed-shell species is considered to be reliable if the T_1 diagnostic value is within 0.020. For open-shell systems, a higher threshold value for the T_1 diagnostic up to 0.044 can be acceptable.[38,39] For all the species during open-shell CCSD(T) calculations, it is found that all T_1 diagnostics values are within 0.030 except for the TSs of allene and 1,3-butene, the values of which are close to 0.039. Thus, the employed single-reference methods are adequate in this work.

https://doi.org/10.1021/acsomega.1c06683
ACS Omega 2022, 7, 8675−8685

Geometry optimization, frequency analysis, and CCSD(T) calculations are performed by using Gaussian 09 software,[40] while DLPNO-CCSD(T) and CCSD(T)-F12 calculations are carried out by using the ORCA 4.2 software.[41,42]

2.3. Reaction Rate. High-pressure limiting rate constants as a function of temperature are computed from canonical TST via MultiWell software.[43−45] The quantum mechanical tunneling corrections are included by using an unsymmetrical Eckart barrier model.[46] It is worth noting that the van der Waals complexes can be formed in the entrance and exit channels for the studied reaction class. To this end, it is necessary to include the contribution of the complexes to the rate constant. However, a series of previous studies indicated that the formation of the reactant complexes is not the rate-determining step.[47−49] Such a simplification is rational in kinetics because the energies of the formed weakly complexes are just lower than those of the reactants and are rather unstable at high temperatures. Hence, it is fairly reasonable to employ the TST method regardless of the van der Waals complexes to estimate the high-pressure limit rate constants. The rate constants are computed at temperatures from 500 to 2000 K in increments of 100 K and are fitted into the modified Arrhenius equation as $k(T) = AT^n \exp(-E_a/RT)$ in which A is the Arrhenius prefactor, E_a is the barrier height, and n is the temperature exponent representing the deviation from the standard Arrhenius equation.

2.4. Kinetic Modeling. The fitted rate coefficients in this work are incorporated into the recently released skeletal NUI GMECH 1.1 base model because it is fundamentally developed based on several prior studies widely used in the combustion community.[5] The recently released NUIGMECH 1.1 base model incorporates recent advances in rate constants and thermodynamic properties through the critical evaluation of newly published experimental and theoretical studies and has been tested against various validation targets, including ignition delay times, burning velocities, and intermediate species of important fuels obtained from a number of recent literature studies.[5,14−16,21] The updated model can reproduce all of the existing experimentally observed data describing combustion characteristics under a variety of pressures, temperatures, and mixture compositions. The computed rate constants are first compared with previously used rate constants in detailed mechanisms. Then, the ignition delay times for typical fuels are predicted by using the original and updated mechanisms. Kinetic modeling for ignition and pyrolysis is performed by using Cantera software.[50]

3. RESULTS AND DISCUSSION

3.1. Benchmarking Energy Results. To facilitate comparison of various theoretical methods, the three reactions, i.e., $H_2 + CH_3O_2 = H + CH_3OOH$, $CH_4 + CH_3O_2 = CH_3 + CH_3OOH$, and $C_2H_4 + CH_3O_2 = C_2H_3 + CH_3OOH$, are used for benchmark purpose. Table 1 lists the computed reaction energy barriers and enthalpies for the three reactions at different levels of theory. For the barrier of reaction $CH_4 + CH_3O_2 = CH_3 + CH_3OOH$, Hashemi et al.[19] used a high-level method at the CCSD(T)-F12/CBS level in combination with a series of corrections to derive an accurate barrier with a value of 25.29 kcal/mol. It can be seen that the present values for this reaction derived at CCSD(T)/cc-pVTZ, CCSD(T)/cc-pVQZ, CCSD(T)-F12/cc-pVTZ-F12, and CCSD(T)/CBS-(tz,qz) are very close to the recommended value of 25.29 kcal/mol. Although the B2PLYP-D3/cc-pVTZ method has been shown to be effective for geometry optimization and frequency analysis,[27] this method tends to underestimate the energy barriers compared with the CCSD(T) method. Further, the MP2/cc-pVTZ method is also not suitable for energy calculations. Without any basis set extrapolation, the explicit CCSD(T)-F12 method with a cc-pVTZ-F12 basis set can achieve accuracy at the CCSD(T)/cc-pVQZ level. The linear-scaling DLPNO-CCSD(T) method with cc-pVQZ or def2-QZVPP basis sets also exhibits good performance for this reaction class and thus can be recommended for the study of large reaction systems. Using the results from CCSD(T)/CBS(tz,qz) and CCSD(T)-F12/cc-pVTZ-F12 methods for the three reactions as benchmark values, it can be seen that the CCSD(T)-MP2/CBS(dz,tz) method outperforms the other methods at a comparative computational cost. The CCSD(T) method with a large cc-pVQZ basis set can achieve good accuracy, but the computational cost is relatively larger. Thus, the CCSD(T)-MP2/CBS(dz,tz) method is used for the comparative and hierarchical study of the titled reaction class at the same level.

Table 1. Computed Energy Barriers and Reaction Enthalpies for $H_2 + CH_3O_2 = H + CH_3OOH$, $CH_4 + CH_3O_2 = CH_3 + CH_3OOH$, and $C_2H_4 + CH_3O_2 = C_2H_3 + CH_3OOH$ All energies are in kcal/mol and include B2PLYP-D3/cc-pVTZ ZPE correction.

theoretical method	$H_2 + CH_3O_2$		$CH_4 + CH_3O_2$		$C_2H_4 + CH_3O_2$	
	ΔE	$\Delta_r H_0^0$	ΔE	$\Delta_r H_0^0$	ΔE	$\Delta_r H_0^0$
B2PLYP-D3/cc-pVTZ	23.98	21.21	24.16	21.03	23.96	26.98
MP2/cc-pVTZ	20.65	9.09	21.75	13.05	26.48	24.84
CCSD(T)/cc-pVDZ	26.67	19.66	26.73	21.15	26.20	27.18
CCSD(T)/cc-pVTZ	25.87	19.15	25.34	19.01	25.22	25.31
CCSD(T)/cc-pVQZ	25.53	18.70	25.18	18.55	25.20	24.83
CCSD(T)/CBS(tz,qz)	25.29	18.39	25.07	18.24	25.18	24.50
CCSD(T)-MP2/CBS(dz,tz)	25.17	18.39	24.90	18.07	25.21	24.58
DLPNO-CCSD(T)/cc-pVTZ	26.12	19.02	25.65	18.86	25.49	25.00
DLPNO-CCSD(T)/cc-pVQZ	25.66	18.40	25.45	18.32	25.41	24.42
DLPNO-CCSD(T)/def2-TZVPP	26.17	18.83	25.76	18.54	25.81	24.76
DLPNO-CCSD(T)/def2-QZVPP	25.56	18.27	25.35	18.10	25.41	24.27
CCSD(T)-F12/cc-pVTZ-F12	25.44	18.73	25.16	18.50	25.18	24.72

3.2. Energy Results for C_1−C_4 Hydrocarbons. Table 2 lists the computed reaction energy barriers and enthalpies for the studied reactions at the CCSD(T)-MP2/CBS//uB2PLYP-D3/cc-pVTZ level of theory. For reaction enthalpies, it can be seen that all the computed values are positive except for R18 with a slightly negative value, indicating that the abstraction reaction class is endothermic. The energy barriers and enthalpies are significantly affected by the molecular structures. Although H_2 is an important reactive fuel, the abstraction by CH_3O_2 is not easy to occur as revealed from the computed barriers and enthalpies. The energy barriers for H_2, CH_4, and

https://doi.org/10.1021/acsomega.1c06683
ACS Omega 2022, 7, 8675−8685

Table 2. Computed Reaction Energy Barriers and Enthalpies for the Studied Reactions at the CCSD(T)-MP2/CBS//uB2PLYP-D3/cc-pVTZ Level of Theory All energies are in kcal/mol and include B2PLYP-D3/cc-pVTZ ZPE correction.

molecule	no.	reactions	ΔE	$\Delta_f H_0^0$
hydrogen	R1	$H_2 + CH_3O_2 = H + CH_3OOH$	25.17	18.39
methane	R2	$CH_4 + CH_3O_2 = CH_3 + CH_3OOH$	24.90	18.07
ethylene	R3	$C_2H_4 + CH_3O_2 = C_2H_3 + CH_3OOH$	25.21	24.58
ethane	R4	$C_2H_6 + CH_3O_2 = C_2H_5 + CH_3OOH$	20.33	14.37
propene	R5	$CH_2{=}CHCH_3 + CH_3O_2 = {\bullet}HC{=}CHCH_3 + CH_3OOH$	25.16	25.81
	R6	$CH_2{=}CHCH_3 + CH_3O_2 = CH_2{=}C{\bullet}CH_3 + CH_3OOH$	22.17	29.02
	R7	$CH_2{=}CHCH_3 + CH_3O_2 = CH_2{=}CHCH_2{\bullet} + CH_3OOH$	16.54	1.92
propane	R8	$CH_3CH_2CH_3 + CH_3O_2 = CH_3CH_2CH_2{\bullet} + CH_3OOH$	20.26	14.75
	R9	$CH_3CH_2CH_3 + CH_3O_2 = CH_3CH{\bullet}CH_3 + CH_3OOH$	17.34	11.75
allene	R10	$CH_2{=}C{=}CH_2 + CH_3O_2 = {\bullet}HC{=}C{=}CH_2 + CH_3OOH$	18.84	4.82
n-butane	R11	$CH_3(CH_2)_2CH_3 + CH_3O_2 = CH_3(CH_2)_2CH_2{\bullet} + CH_3OOH$	20.14	14.73
	R12	$CH_3(CH_2)_2CH_3 + CH_3O_2 = CH_3CH{\bullet}CH_2CH_3 + CH_3OOH$	17.05	12.09
iso-butane	R13	$(CH_2)_3CH + CH_3O_2 = (CH_3)_2CHCH_2{\bullet} + CH_3OOH$	19.81	15.19
	R14	$(CH_2)_3CH + CH_3O_2 = (CH_3)_3C{\bullet} + CH_3OOH$	15.06	10.21
1-butene	R15	$CH_2{=}CHCH_2CH_3 + CH_3O_2 = {\bullet}CH{=}CHCH_2CH_3 + CH_3OOH$	24.80	25.63
	R16	$CH_2{=}CHCH_2CH_3 + CH_3O_2 = CH_2{=}C{\bullet}CH_2CH_3 + CH_3OOH$	21.69	21.85
	R17	$CH_2{=}CHCH_2CH_3 + CH_3O_2 = CH_2{=}CHCH_2CH_2{\bullet} + CH_3OOH$	20.49	15.04
	R18	$CH_2{=}CHCH_2CH_3 + CH_3O_2 = CH_2{=}CHCH{\bullet}CH_3 + CH_3OOH$	14.65	−0.70
2-butene	R19	$CH_3CH{=}CHCH_3 + CH_3O_2 = CH_3CHCHCH_2{\bullet} + CH_3OOH$	15.60	1.58
	R20	$CH_3CH{=}CHCH_3 + CH_3O_2 = CH_3CH{=}C{\bullet}CH_3 + CH_3OOH$	22.10	22.39
iso-butene	R21	$CH_2{=}C(CH_3)_2 + CH_3O_2 = CH_2{=}C(CH_2{\bullet})CH_3 + CH_3OOH$	16.59	3.31
	R22	$CH_2{=}C(CH_3)_2 + CH_3O_2 = {\bullet}CH{=}C(CH_3)_2 + CH_3OOH$	25.14	26.28
1,3-butadiene	R23	$CH_2{=}CHCH{=}CH_2 + CH_3O_2 = CH_2{=}CHCH{=}CH{\bullet} + CH_3OOH$	27.20	27.90
	R24	$CH_2{=}CHCH{=}CH_2 + CH_3O_2 = CH_2{=}CHC{\bullet}{=}CH_2 + CH_3OOH$	24.52	24.81
propyne	R25	$HC{\equiv}CCH_3 + CH_3O_2 = HC{\equiv}CCH_2{\bullet} + CH_3OOH$	18.21	5.96
1-butyne	R26	$HC{\equiv}CCH_2CH_3 + CH_3O_2 = HC{\equiv}CCH_2CH_2{\bullet} + CH_3OOH$	20.71	15.61
	R27	$HC{\equiv}CCH_2CH_3 + CH_3O_2 = HC{\equiv}CCH{\bullet}CH_3 + CH_3OOH$	15.62	3.03
2-butyne	R28	$CH_3C{\equiv}CCH_3 + CH_3O_2 = CH_3C{\equiv}CCH_2{\bullet} + CH_3OOH$	16.93	5.22

C_2H_4 are very close to each other. For saturated hydrocarbons including C_2H_6, C_3H_8, *n*-butane, and iso-butane, it can be seen that the energy barriers of the abstraction reactions at the primary C−H site are the largest with values around 20 kcal/mol followed by the abstract at the secondary C−H site with values around 17 kcal/mol, and the abstraction at the tertiary C−H site is the easiest with the smallest barriers around 15 kcal/mol. The reactivity trend of this abstraction class is generally in good consistent with the other abstraction reaction classes, i.e., by H, CH_3, OH, and HO_2 radicals.[8,18,51]

For unsaturated hydrocarbons with one double C=C bond including C_2H_4, propene, 1-butene, 2-butene, and iso-butene, the abstraction reactions at the two C=C double bond positions are still affected by the structural effect. Generally, the abstraction at the CH_2 group in the C=C double bond (the primary vinylic carbon site) shows a larger energy barrier with a value around 25 kcal/mol, while the abstraction at the position with substitution in the C=C double bond shows a smaller value around 22 kcal/mol. It is worth noting that the abstraction reaction at the primary vinylic carbon site can show *cis* and *trans* configurations due to the location of the C=C double bond,[48] and Table 2 only lists the energies with the smaller barriers. However, the differences of the energy barriers between the values of *cis* and *trans* configurations are very small. For the other positions in these fuels, it can be seen that the energy barrier of the reaction at the secondary allylic carbon site (R18) with a value of 14.65 kcal/mol is smaller than that at the primary allylic sites (i.e., R7, R19, and R21) with values around 16 kcal/mol. The abstraction reaction at a position not directly connected to the C=C double bond (R17) is hardly affected. For 1,3-butadiene, the energy barriers of the abstractions at the two reaction sites are generally larger than those of the abstractions in molecules with a single C=C double bond by 2 kcal/mol, respectively, which is probably induced by the steric effect.

For the abstraction reactions of propyne and butyne, abstractions at the C≡C site are very difficult due to the large bond energies.[52] Therefore, only abstraction reactions at the propargyl site are studied. The reactivity trends at different propargyl sites are very similar to those of alkenes. Specifically, the energy barrier at the primary propargyl site is larger than that at the secondary propargyl site by about 1−2 kcal/mol, while the reaction at a position not directly connected to the C≡C bond is still hardly affected. As an important isomer of propyne, the abstraction reaction for allene is also studied as shown in Table 2. The energy barrier of R10 is close to that of R25 at the propargyl site in propyne, but it is much smaller than that of abstraction reactions at vinylic sites in alkene with one C=C double bond. Overall, the computed results for the studied reaction class reveal that the energy barriers at the same types of carbon atoms in the molecules are close to each other, and the reactivity trends are also in good consistent with previous studies.[17,18,48,52,53]

3.3. Rate Constants. The high-pressure limiting rate constants of the studied abstraction reactions are all computed by using canonical TST with 1-D hindered rotor approximations for the treatment of internal rotations. The Fourier series are used for fitting the scanned results of international rotations. To obtain rate constants with hierarchical consistency, the energy information computed at the CCSD(T)-MP2/CBS//uB2PLYP-D3/cc-pVTZ level is employed. The computed rate constants in this work are first compared with available literature data as shown in Figures 1 and 2. For the abstraction reaction of CH_4 with CH_3O_2, the computed rate constants in this work are in good consistent with the results by Hashemi et al.[19] at low temperatures, while slight large deviations are observed under high-temperature conditions above 1000 K. As discussed previously, the computed energy barrier of this reaction is very close to that reported by Hashemi et al.,[19] and thus, the computed rate constants at low temperatures are close to those reported by Hashemi et al.[19] because the rate constants at low temperatures are mainly controlled by enthalpy. However, under high-temperature

https://doi.org/10.1021/acsomega.1c06683
ACS Omega 2022, 7, 8675−8685

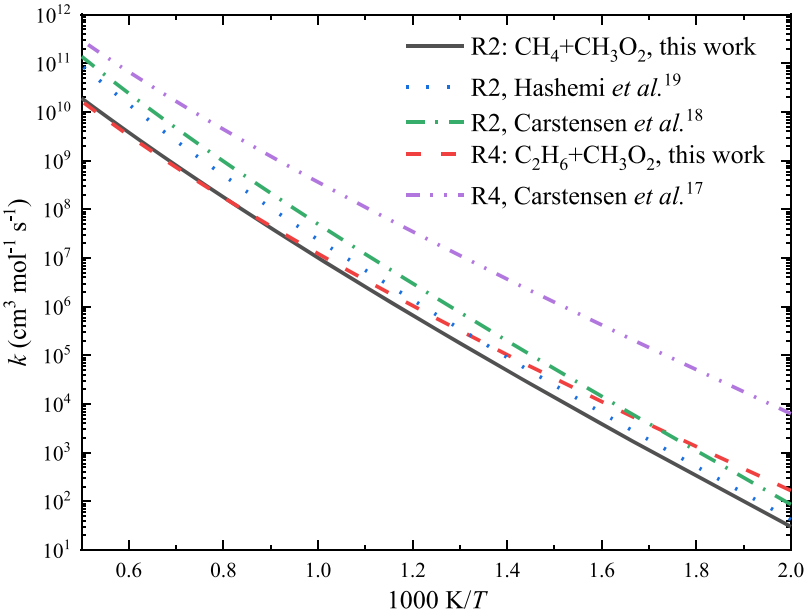

Figure 1. Computed rate constants for R2 and R4 with available literature data.

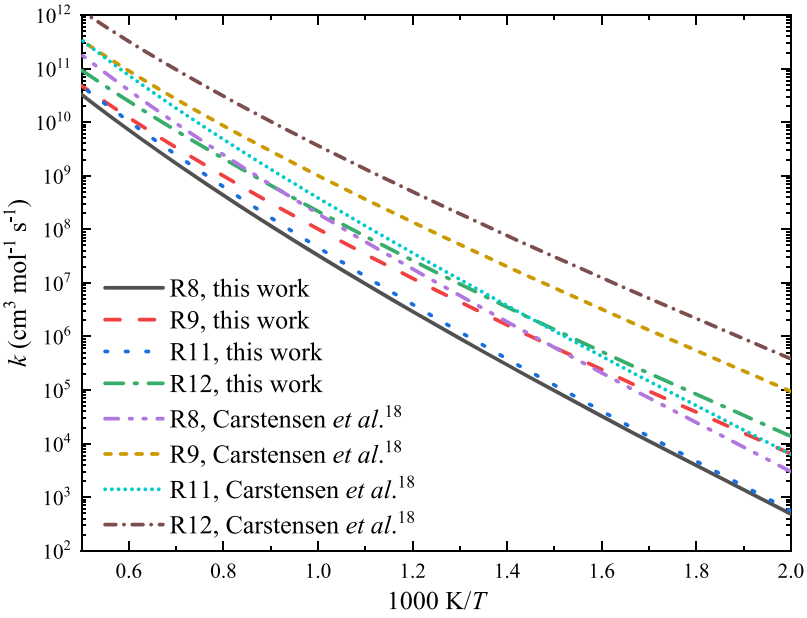

Figure 2. Computed rate constants for abstraction reactions of propane and *n*-butane by CH_3O_2 with available literature data.

conditions, the entropy changes significantly affect the computed rate constants, which is much relevant to the frequency analysis results. The deviations between this study and Hashemi et al.[19] at high temperatures can be attributed to the different frequency analysis methods. The rate constants derived by Carstensen et al.[18] at the CBS-QB3 level tend to be larger compared with this work and Hashemi et al.[19] Both the computed energy barrier and frequency results exhibit large influence on the computed results. The uncertainty of the energy information from CBS-QB3 tends to be larger than the other methods; thus, it is expected that a large uncertainty exists for the results by Carstensen et al.[18] It can be seen that the results for R4, i.e., abstraction reaction of ethane with CH_3O_2, by Carstensen et al.[18] are also significantly higher than those of the present work. Similar trends are also found for abstraction reactions of propane and *n*-butane as shown in Figure 2. However, the reactivity of the secondary and primary abstraction sites can be reflected correctly using different methods, and the rate constants of abstraction reactions at the secondary site are significantly higher than those at the primary site.

In order to get a comprehensive and hierarchical comparison of structural effect on the abstraction reactions, Figures 3 and 4 display the computed rate constants as a function of temperature for saturated and unsaturated hydrocarbons studied in this work. From Figure 3, it is observed that the reaction rate constants of methane with CH_3O_2 are the lowest, especially under lower-temperature conditions. The reaction rate constants generally exhibit the following trend: the rate constants at the tertiary site are larger than those at the secondary site, and the rate constants at the primary site are the lowest, which are in accordance with the computed energy

https://doi.org/10.1021/acsomega.1c06683
ACS Omega 2022, 7, 8675−8685

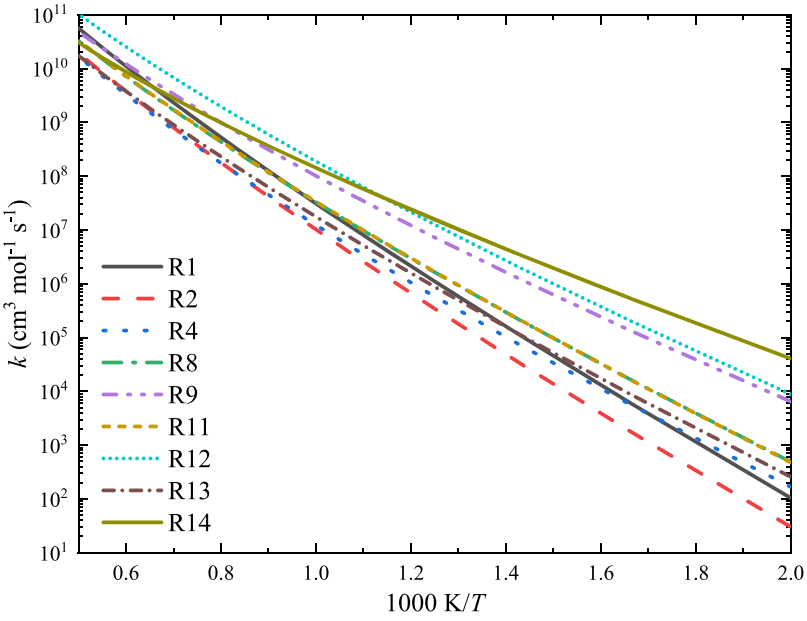

Figure 3. Structural effect on the rate constants for abstraction reactions of saturated hydrocarbons by CH_3O_2.

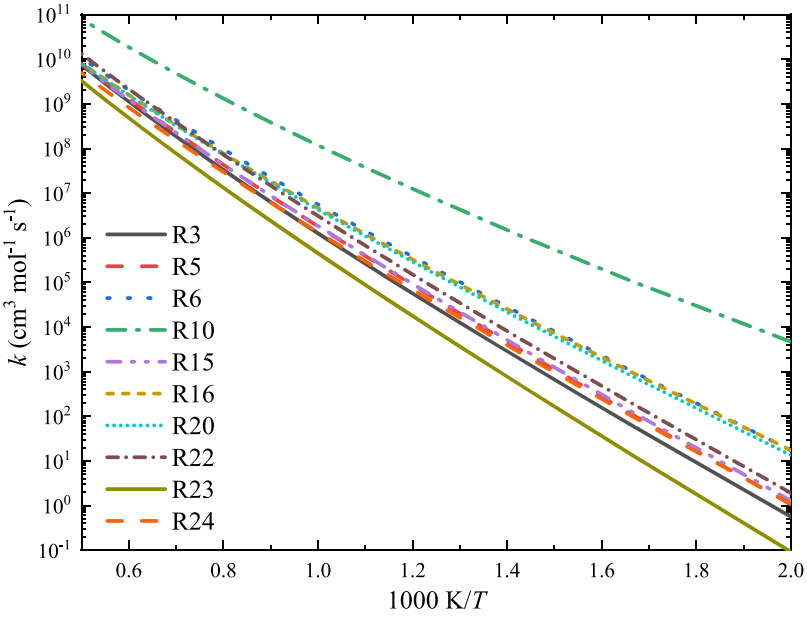

Figure 4. Structural effect on the rate constants for abstraction reactions of unsaturated hydrocarbons at the C=C double bond sites by CH_3O_2.

barriers. The structural effect on the primary and secondary reaction sites is small; i.e., the rate constants of reactions R9 and R12 at the primary sites and the rate constants of reactions R4, R8, R11, and R13 at the secondary sites are close to each other. The rate constants of the abstraction reaction R1 are very close to the results of ethane with CH_3O_2 and slightly larger than those of methane with CH_3O_2.

Figure 4 shows the rate constants as a function of temperature for the abstraction reactions at the C=C double bond sites to demonstrate the structural effect on the primary and secondary vinylic sites. The abstraction reaction of allene with CH_3O_2 is also explicitly shown for comparison. It can be seen that the rate constants of the abstraction reaction of allene are significantly larger than those at the single C=C double bond, indicating the higher reactivity of allene under the studied temperatures. Besides the two abstraction reactions of 1,3-butadiene, the rate constants at the secondary vinylic site are generally larger than those at the primary vinylic site, especially at lower temperatures. Similarly, the rate constants at the primary vinylic and secondary vinylic sites are close to each other, respectively, indicating that the structural effect on the C=C double bond sites is small. It is shown that the rate constants of the abstraction reactions at the primary and secondary vinylic sites in 1,3-butadiene are lower than those of the corresponding reactions in molecules with a single C=C double bond, which is confirmed by the computed energy barriers. Thus, the rate constants used in kinetic models for 1,3-butadiene should be treated separately and also highlight the importance of the present work to perform a hierarchical study of this reaction class.

As shown from the computed energy barriers and reaction enthalpies, the abstraction reactions at the allylic or propargyl

https://doi.org/10.1021/acsomega.1c06683
ACS Omega 2022, 7, 8675−8685

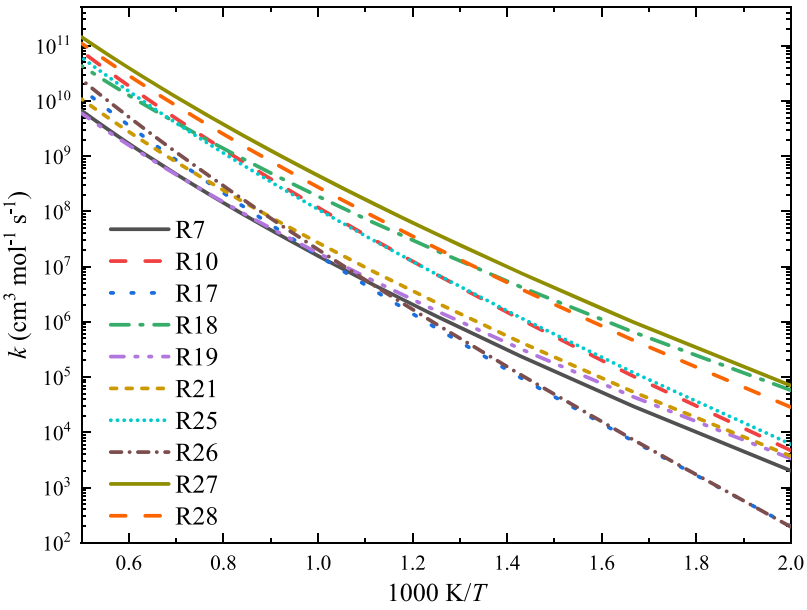

Figure 5. Structural effect on the rate constants for abstraction reactions of unsaturated hydrocarbons by CH_3O_2.

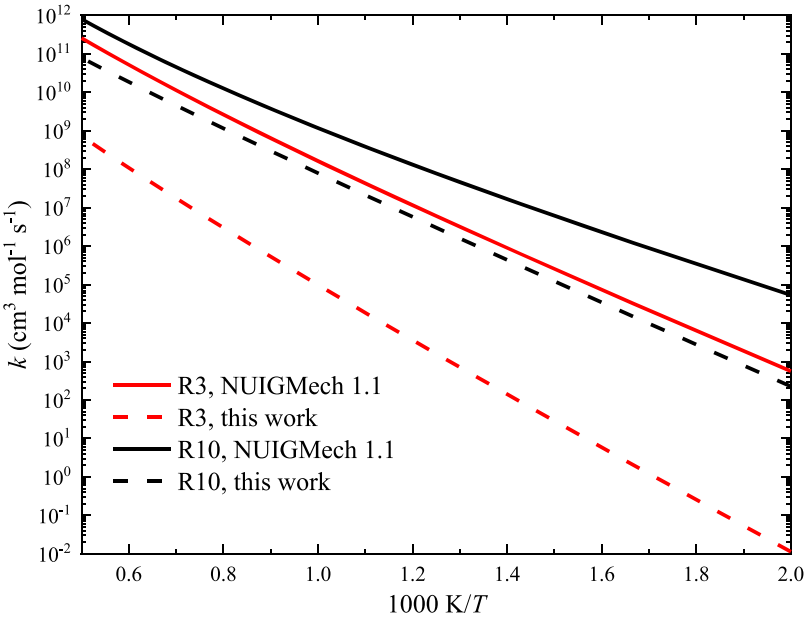

Figure 6. Comparisons of computed rate constants for R3 and R10 with those used in the previous NUIGMech 1.1 mechanism.

sites should be dominant for unsaturated hydrocarbons. Figure 5 shows the rate constants as a function of temperature at various reaction sites except for those at the C═C/C≡C sites for the studied unsaturated hydrocarbons. For the studied alkenes, the rate constants of reactions R7, R19, and R21 at the primary allylic site are close to each other, indicating that the structural effect on this site can be neglected due to the blocking effect of the C═C double bond. The rate constants of abstraction reactions at the primary allylic site are much lower than those at the secondary allylic site (R18). Similar to alkenes, the reactivity at different reaction sites for alkyne exhibits a similar trend; i.e., the rate constants at the secondary propargyl site (R27) are larger than those at the primary sites (R25 and R28). The reactivity trend is also in good correlation with previous studies.[52] However, the rate constants at the propargyl sites in propyne and 2-butyne still exhibit large differences as shown by the computed barriers. For the two isomers of C_3H_4, it is interesting to observe that the abstraction rate constants at the propargyl site in propyne and in allene are nearly identical to each other. From Figure 5, it is also found that the rate constants at the two primary sites (R17 in 1-butene and R26 in 1-butyne) are close to each other, and the results are also nearly identical to those at the primary site in *n*-butane (R11), indicating that the unsaturated C═C/C≡C bonds hardly affect the reactivity of reaction sites with separations. Overall, the rate constants of the corresponding propargyl site are larger than that of the allylic site, which is larger than that of the saturated carbon site in order.

3.4. Kinetic Modeling. To facilitate kinetic modeling studies, the computed rate constants are fitted into the modified Arrhenius format as shown in Table 3. First, the fitted rate constants are compared with those used in previously

https://doi.org/10.1021/acsomega.1c06683
ACS Omega 2022, 7, 8675−8685

Table 3. Fitted Rate Coefficients in the Modified Arrhenius Format for the Abstraction Reactions at the CCSD(T)-MP2/CBS//uB2PLYP-D3/cc-pVTZ Level (AT^n in cm^3 mol^{-1} s^{-1}; E_a in cal mol^{-1})

no.	reactions	A	n	E_a
R1	$H_2 + CH_3O_2 = H + CH_3OOH$	2.33×10^3	2.96	21,800
R2	$CH_4 + CH_3O_2 = CH_3 + CH_3OOH$	6.06×10^3	2.72	22,500
R3	$C_2H_4 + CH_3O_2 = C_2H_3 + CH_3OOH$	1.53×10^4	2.65	28,104
R4	$C_2H_6 + CH_3O_2 = C_2H_5 + CH_3OOH$	2.52×10^9	1.18	28,112
R5	$CH_2{=}CHCH_3 + CH_3O_2 = \bullet HC{=}CHCH_3 + CH_3OOH$	7.63×10^4	2.42	27,330
R6	$CH_2{=}CHCH_3 + CH_3O_2 = CH_2{=}C\bullet CH_3 + CH_3OOH$	2.47×10^8	1.41	27,749
R7	$CH_2{=}CHCH_3 + CH_3O_2 = CH_2{=}CHCH_2\bullet + CH_3OOH$	4.53×10^6	1.66	21,226
R8	$CH_3CH_2CH_3 + CH_3O_2 = CH_3CH_2CH_2\bullet + CH_3OOH$	5.31×10^9	1.11	26,289
R9	$CH_3CH_2CH_3 + CH_3O_2 = CH_3CH\bullet CH_3 + CH_3OOH$	9.55×10^7	1.54	21,711
R10	$CH_2{=}C{=}CH_2 + CH_3O_2 = \bullet HC{=}C{=}CH_2 + CH_3OOH$	3.36×10^8	1.49	23,325
R11	$CH_3(CH_2)_2CH_3 + CH_3O_2 = CH_3(CH_2)_2CH_2\bullet + CH_3OOH$	2.25×10^2	3.10	18,997
R12	$CH_3(CH_2)_2CH_3 + CH_3O_2 = CH_3CH\bullet CH_2CH_3 + CH_3OOH$	3.10×10^8	1.50	22,369
R13	$(CH_2)_3CH + CH_3O_2 = (CH_3)_2CHCH_2\bullet + CH_3OOH$	2.85×10^9	1.11	26,240
R14	$(CH_2)_3CH + CH_3O_2 = (CH_3)_3C\bullet + CH_3OOH$	2.91×10^4	2.37	16,386
R15	$CH_2{=}CHCH_2CH_3 + CH_3O_2 = \bullet CH{=}CHCH_2CH_3 + CH_3OOH$	5.02×10^4	2.46	26,887
R16	$CH_2{=}CHCH_2CH_3 + CH_3O_2 = CH_2{=}C\bullet CH_2CH_3 + CH_3OOH$	1.84×10^8	1.41	27,423
R17	$CH_2{=}CHCH_2CH_3 + CH_3O_2 = CH_2{=}CHCH_2CH_2\bullet + CH_3OOH$	2.76×10^9	1.11	26,366
R18	$CH_2{=}CHCH_2CH_3 + CH_3O_2 = CH_2{=}CHCH\bullet CH_3 + CH_3OOH$	3.35×10^9	1.02	20,632
R19	$CH_3CH{=}CHCH_3 + CH_3O_2 = CH_3CH{=}CHCH_2\bullet + CH_3OOH$	1.71×10^6	1.73	20,000
R20	$CH_3CH{=}CHCH_3 + CH_3O_2 = CH_3CH{=}C\bullet CH_3 + CH_3OOH$	1.88×10^8	1.41	27,700
R21	$CH_2{=}C(CH_3)_2 + CH_3O_2 = CH_2{=}C(CH_2\bullet)CH_3 + CH_3OOH$	5.44×10^6	1.69	20,849
R22	$CH_2{=}C(CH_3)_2 + CH_3O_2 = \bullet CH{=}C(CH_3)_2 + CH_3OOH$	1.10×10^5	2.44	27,198
R23	$CH_2{=}CHCH{=}CH_2 + CH_3O_2 = CH_2{=}CHCH{=}CH\bullet + CH_3OOH$	1.92×10^8	1.46	32,866
R24	$CH_2{=}CHCH{=}CH_2 + CH_3O_2 = CH_2{=}CHC\bullet{=}CH_2 + CH_3OOH$	2.23×10^4	2.50	26,462
R25	$HC{\equiv}CCH_3 + CH_3O_2 = HC{\equiv}CCH_2\bullet + CH_3OOH$	1.81×10^8	1.51	22,540
R26	$HC{\equiv}CCH_2CH_3 + CH_3O_2 = HC{\equiv}CCH_2CH_2\bullet + CH_3OOH$	4.35×10^9	1.11	26,829
R27	$HC{\equiv}CCH_2CH_3 + CH_3O_2 = HC{\equiv}CCH\bullet\ CH_3 + CH_3OOH$	1.29×10^8	1.58	19,887
R28	$CH_3C{\equiv}CCH_3 + CH_3O_2 = CH_3C{\equiv}CCH_2\bullet + CH_3OOH$	1.36×10^8	1.57	20,950

developed kinetic models to demonstrate their differences. Then, we implement the fitted rate coefficients into the developed NUIGMech 1.1 models and perform kinetic modeling of autoignition characteristics for typical hydrocarbons to demonstrate the accuracy of rate constants of this reaction class on kinetic modeling results. It is worth noting that the previous detailed kinetic models have been optimized to match experimental results. Therefore, comparisons with experimental results are not compared because they are affected by too many reactions in the detailed kinetic models. Here, the major purpose is to show the effect of the studied reaction class on kinetic modeling results.

Figure 6 shows a comparison of some reaction rate constants computed in this work and those used in previously detailed mechanisms by analogy or estimation. It can be seen that the computed rate constants demonstrate large deviations for typical reactions. Figure 7 shows the modeling results of ignition delay time of methane and allene at 10 bar with an equivalence ratio of 1.0. It is shown that the studied reaction class exhibits large effects on ignition under low-temperature conditions. For the other fuels, the ignition delay time is not very sensitive to the studied reactions, and the ignitions are very close to each other. After detailed comparisons with the reactions used in the previous NUIGMech 1.1 mechanism, we found that for most of the large fuels, the rate constants still exhibit large deviations compared with the present work. In particular, the abstraction reactions for propene and butene at the C=C double bond are neglected, which should be avoided to develop a comprehensive mechanism. Figure 8 demonstrates the branching ratio analysis of the three abstraction reactions by CH_3O_2 of propene as a function of temperature. It can be seen that although the abstraction at the allylic site is dominant under low-temperature conditions, the two abstraction reactions at the C=C double bond tend to increase as the temperature increases, and the total contributions can reach a maximum value of around 0.75. Thus, all the abstraction reactions should be included.

4. CONCLUSIONS

This work reports a systematic and hierarchical ab initio and chemical kinetic study of the abstraction reactions of H_2/C_1-C_4 hydrocarbons by the methyl peroxy radical (CH_3O_2). The hydrocarbon fuels include hydrogen, alkanes, alkenes, and alkynes with a carbon number from 1 to 4. The B2PLYP-D3/cc-pVTZ level of theory is employed to optimize the geometries of all of the reactants, TSs, and products and also the treatments of hindered rotation for lower frequency modes. We performed benchmark calculations for the energy barriers and enthalpies of typical reactions to select and recommend suitable theoretical methods for the studied reaction class. It is shown that the basis set exhibits a large effect using different accurate couple cluster methods, and the CCSD(T) method should be used at least in combination with the cc-pVTZ basis set to obtain reliable energies. To get hierarchical and consistent rate constants used for kinetic models, the reaction energy information is calculated using the CCSD(T) method with basis extrapolations. Based on the quantum chemistry calculations, reaction rate constants are computed via conventional TST with quantum tunneling corrections. Structural effects on the reaction energy and rate constants are systematically analyzed. The calculated rate constants are further implemented into the recently developed NUIGMECH1.1 base model for kinetic modeling of ignition properties. The ignition delay times are affected for some fuels. Further, a detailed comparison of the previous reactions used in kinetic models and the present work highlights the importance of the present work to obtain accurate reaction rate constants for the studied reaction class.

https://doi.org/10.1021/acsomega.1c06683
ACS Omega 2022, 7, 8675−8685

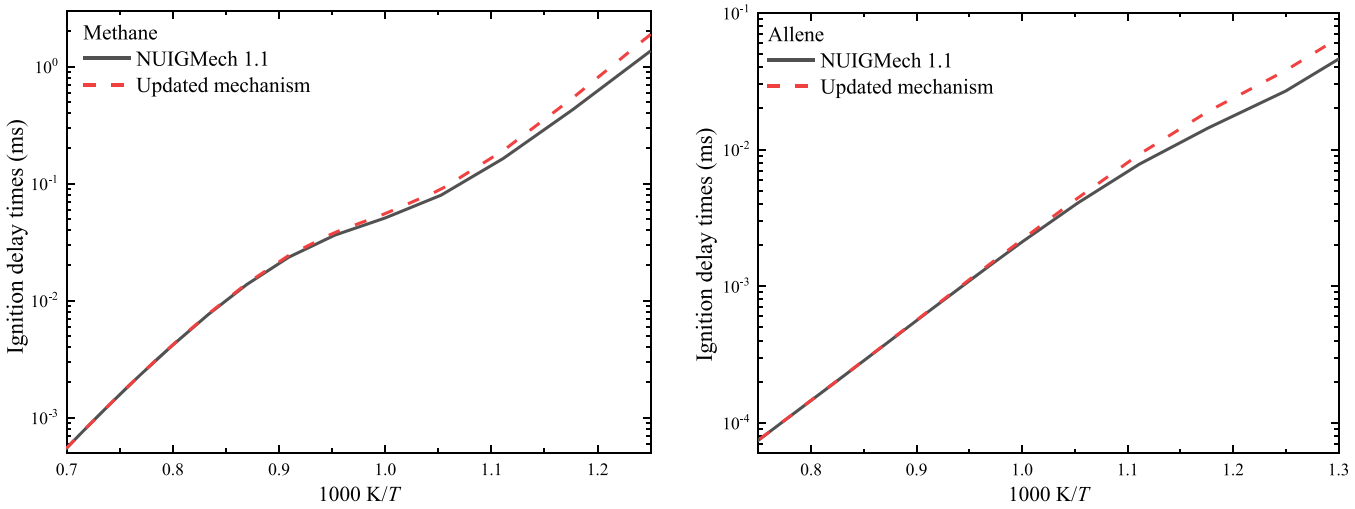

Figure 7. Ignition delay time simulation results using the skeletal NUIGMech 1.1 and updated mechanism with the present rate constants.

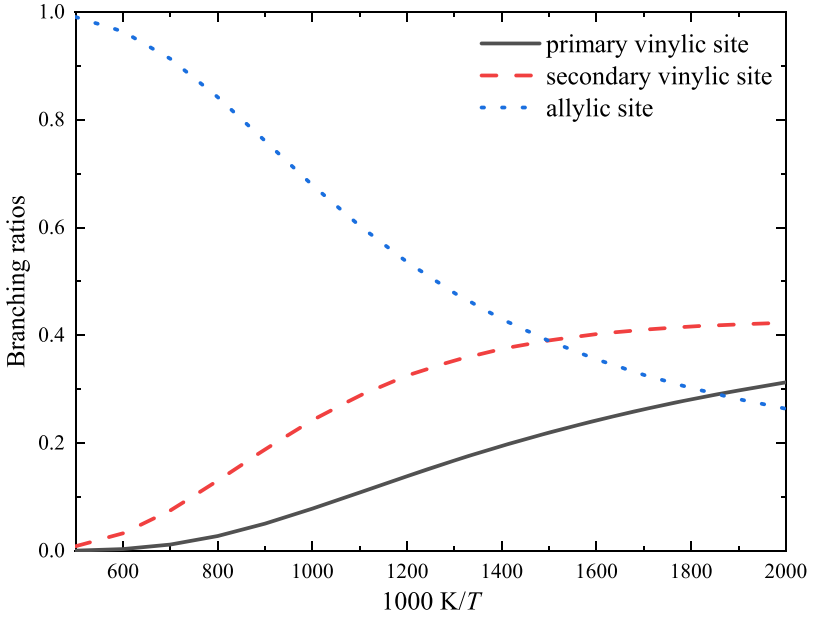

Figure 8. Branching ratios of the three abstraction reactions by CH_3O_2 of propene.

■ ASSOCIATED CONTENT

Supporting Information

The Supporting Information is available free of charge at https://pubs.acs.org/doi/10.1021/acsomega.1c06683.

Optimized geometries; frequency analysis results; IRC plots; computed energy information; and relaxed potential energy scan results (PDF)

Updated NUIGMech mechanism results (ZIP)

■ AUTHOR INFORMATION

Corresponding Authors

Jinhu Liang − *Faculty of Materials and Chemical Engineering, Yibin University, Yibin, Sichuan 644000, People's Republic of China; School of Environment and Safety Engineering, North University of China, Taiyuan 030051, People's Republic of China;* orcid.org/0000-0003-3972-7664; Email: jhliang@nuc.edu.cn

Quan-De Wang − *Jiangsu Key Laboratory of Coal-Based Greenhouse Gas Control and Utilization, Low Carbon Energy Institute, China University of Mining and Technology, Xuzhou 221008, People's Republic of China;* orcid.org/0000-0002-3941-0192; Email: quandewang@cumt.edu.cn

Authors

Shenying Xu − *Faculty of Materials and Chemical Engineering, Yibin University, Yibin, Sichuan 644000, People's Republic of China*

Shutong Cao − *School of Environment and Safety Engineering, North University of China, Taiyuan 030051, People's Republic of China*

Ruining He − *School of Environment and Safety Engineering, North University of China, Taiyuan 030051, People's Republic of China*

Guoliang Yin − *Faculty of Materials and Chemical Engineering, Yibin University, Yibin, Sichuan 644000, People's Republic of China*

Complete contact information is available at: https://pubs.acs.org/10.1021/acsomega.1c06683

https://doi.org/10.1021/acsomega.1c06683
ACS Omega 2022, 7, 8675−8685

Notes

The authors declare no competing financial interest.

■ ACKNOWLEDGMENTS

The work was supported by the National Natural Science Foundation of China (12172335). We also thank National Supercomputing Center in Shenzhen for providing the computational resources and Gaussian 09 suite of programs.

■ REFERENCES

(1) Kohse-Hoinghaus, K. Combustion in the future: The importance of chemistry. *Proc. Combust. Inst.* **2021**, *38*, 1−56.
(2) Curran, H. J. Developing detailed chemical kinetic mechanisms for fuel combustion. *Proc. Combust. Inst.* **2019**, *37*, 57−81.
(3) Wang, Q.-D.; Sun, Y.; Curran, H. J. Comparative Chemical Kinetic Analysis and Skeletal Mechanism Generation for Syngas Combustion with NOX Chemistry. *Energy Fuels* **2020**, *34*, 949−964.
(4) Sarathy, S. M.; Farooq, A.; Kalghatgi, G. T. Recent progress in gasoline surrogate fuels. *Prog. Energy Combust. Sci.* **2018**, *65*, 67−108.
(5) Pelucchi, M.; Cai, L.; Pejpichestakul, W.; Tripathi, R.; Wagnon, S.; Zhang, K.; Raju, M.; Mehl, M.; Faravelli, T.; Pitz, W.; Pitsch, H.; Curran, H.; Senecal, P. K., *Computational Chemistry Consortium: Surrogate Fuel Mechanism Development, Pollutants Sub-Mechanisms and Components Library*, *SAE Technical Paper*, 2019-24-0020.
(6) Battin-Leclerc, F.; Blurock, E.; Bounaceur, R.; Fournet, R.; Glaude, P. A.; Herbinet, O.; Sirjean, B.; Warth, V. Towards cleaner combustion engines through groundbreaking detailed chemical kinetic models. *Chem. Soc. Rev.* **2011**, *40*, 4762−4782.
(7) Wang, H. Formation of nascent soot and other condensed-phase materials in flames. *Proc. Combust. Inst.* **2011**, *33*, 41−67.
(8) Westbrook, C. K.; Curran, H. J. Detailed kinetics of fossil and renewable fuel combustion. In *Mathematical Modelling of Gas-Phase Complex Reaction Systems: Pyrolysis and Combustion*, 2019; pp 363−443.
(9) Zhang, K. W.; Banyon, C.; Bugler, J.; Curran, H. J.; Rodriguez, A.; Herbinet, O.; Battin-Leclerc, F.; B'Chir, C.; Heufer, K. A. An updated experimental and kinetic modeling study of n-heptane oxidation. *Combust. Flame* **2016**, *172*, 116−135.
(10) Hashemi, H.; Christensen, J. M.; Harding, L. B.; Klippenstein, S. J.; Glarborg, P. High-pressure oxidation of propane. *Proc. Combust. Inst.* **2019**, *37*, 461−468.
(11) Mendes, J.; Zhou, C. W.; Curran, H. J. Theoretical Chemical Kinetic Study of the H-Atom Abstraction Reactions from Aldehydes and Acids by <(H)over dot> Atoms and <(H)over dot>, H<(O)over dot>(2), and CH3 Radicals. *J. Phys. Chem. A* **2014**, *118*, 12089−12104.
(12) Mendes, J.; Zhou, C. W.; Curran, H. J. Theoretical Study of the Rate Constants for the Hydrogen Atom Abstraction Reactions of Esters with (OH)-O-center dot Radicals. *J. Phys. Chem. A* **2014**, *118*, 4889−4899.
(13) Wang, Q.-D. Theoretical studies on the hydrogen abstraction reactions of methyl esters with HO_2 radical and the following beta-scission reactions. *J. Phys. Org. Chem.* **2017**, *30*, e3668.
(14) Baigmohammadi, M.; Patel, V.; Martinez, S.; Panigrahy, S.; Ramalingam, A.; Burke, U.; Somers, K. P.; Heufer, K. A.; Pekalski, A.; Curran, H. J. A comprehensive experimental and simulation study of ignition delay time characteristics of single fuel $C_1 - C_2$ hydrocarbons over a wide range of temperatures, pressures, equivalence ratios, and dilutions. *Energy Fuels* **2020**, *34*, 3755−3771.
(15) Baigmohammadi, M.; Patel, V.; Nagaraja, S.; Ramalingam, A.; Martinez, S.; Panigrahy, S.; Mohamed, A. A. E.-S.; Somers, K. P.; Burke, U.; Heufer, K. A.; Pekalski, A.; Curran, H. J. Comprehensive Experimental and Simulation Study of the Ignition Delay Time Characteristics of Binary Blended Methane, Ethane, and Ethylene over a Wide Range of Temperature, Pressure, Equivalence Ratio, and Dilution. *Energy Fuels* **2020**, *34*, 8808−8823.
(16) Ramalingam, A.; Panigrahy, S.; Fenard, Y.; Curran, H.; Heufer, K. A. A chemical kinetic perspective on the low-temperature oxidation of propane/propene mixtures through experiments and kinetic analyses. *Combust. Flame* **2021**, *223*, 361−375.
(17) Carstensen, H.-H.; Dean, A. M. Rate constants for the abstraction reactions $RO^2+C_2H_6$; R=H, CH_3, and C_2H_5. *Proc. Combust. Inst.* **2005**, *30*, 995−1003.
(18) Carstensen, H.-H.; Dean, A. M.; Deutschmann, O. Rate constants for the H abstraction from alkanes (R−H) by $R'O_2$ radicals: A systematic study on the impact of R and R′. *Proc. Combust. Inst.* **2007**, *31*, 149−157.
(19) Hashemi, H.; Christensen, J. M.; Gersen, S.; Levinsky, H.; Klippenstein, S. J.; Glarborg, P. High-pressure oxidation of methane. *Combust. Flame* **2016**, *172*, 349−364.
(20) Wang, H.; Xu, R.; Wang, K.; Bowman, C. T.; Hanson, R. K.; Davidson, D. F.; Brezinsky, K.; Egolfopoulos, F. N. A physics-based approach to modeling real-fuel combustion chemistry - I. Evidence from experiments, and thermodynamic, chemical kinetic and statistical considerations. *Combust. Flame* **2018**, *193*, 502−519.
(21) Wang, Q.-D.; Panigrahy, S.; Yang, S.; Martinez, S.; Liang, J.; Curran, H. J. Development of Multipurpose Skeletal Core Combustion Chemical Kinetic Mechanisms. *Energy Fuels* **2021**, *35*, 6921−6927.
(22) Grimme, S. Semiempirical hybrid density functional with perturbative second-order correlation. *J. Chem. Phys.* **2006**, *124*, 034108.
(23) Grimme, S.; Ehrlich, S.; Goerigk, L. Effect of the Damping Function in Dispersion Corrected Density Functional Theory. *J. Comput. Chem.* **2011**, *32*, 1456−1465.
(24) Kendall, R. A.; Dunning, T. H.; Harrison, R. J. Electron affinities of the first-row atoms revisited. Systematic basis sets and wave functions. *J. Chem. Phys.* **1992**, *96*, 6796−6806.
(25) Becke, A. D. Density-functional thermochemistry. III. The role of exact exchange. *J. Chem. Phys.* **1993**, *98*, 5648−5652.
(26) Zhao, Y.; Truhlar, D. G. The M06 suite of density functionals for main group thermochemistry, thermochemical kinetics, noncovalent interactions, excited states, and transition elements: two new functionals and systematic testing of four M06-class functionals and 12 other functionals. *Theor. Chem. Acc.* **2008**, *120*, 215−241.
(27) Klippenstein, S. J. From theoretical reaction dynamics to chemical modeling of combustion. *Proc. Combust. Inst.* **2017**, *36*, 77−111.
(28) Gonzalez, C.; Schlegel, H. B. Reaction-Path Following in Mass-Weighted Internal Coordinates. *J. Phys. Chem.* **1990**, *94*, 5523−5527.
(29) Watts, J. D.; Gauss, J.; Bartlett, R. J. Coupled-cluster methods with noniterative triple excitations for restricted open-shell Hartree−Fock and other general single determinant reference functions. Energies and analytical gradients. *J. Chem. Phys.* **1993**, *98*, 8718−8733.
(30) Saitow, M.; Becker, U.; Riplinger, C.; Valeev, E. F.; Neese, F. A new near-linear scaling, efficient and accurate, open-shell domain-based local pair natural orbital coupled cluster singles and doubles theory. *J. Chem. Phys.* **2017**, *146*, 164105.
(31) Neese, F.; Atanasov, M.; Bistoni, G.; Maganas, D.; Ye, S. Chemistry and quantum mechanics in 2019: give us insight and numbers. *J. Am. Chem. Soc.* **2019**, *141*, 2814−2824.
(32) Werner, H. J.; Knizia, G.; Manby, F. R. Explicitly correlated coupled cluster methods with pair-specific geminals. *Mol. Phys.* **2011**, *109*, 407−417.
(33) Woon, D. E.; Dunning, T. H. Gaussian basis sets for use in correlated molecular calculations. III. The atoms aluminum through argon. *J. Chem. Phys.* **1993**, *98*, 1358−1371.
(34) Goldsmith, C. F.; Green, W. H.; Klippenstein, S. J. Role of O_2 + QOOH in Low-Temperature Ignition of Propane. 1. Temperature and Pressure Dependent Rate Coefficients. *J. Phys. Chem. A* **2012**, *116*, 3325−3346.
(35) Weigend, F.; Ahlrichs, R. Balanced basis sets of split valence, triple zeta valence and quadruple zeta valence quality for H to Rn: Design and assessment of accuracy. *Phys. Chem. Chem. Phys.* **2005**, *7*, 3297−3305.

https://doi.org/10.1021/acsomega.1c06683
ACS Omega 2022, 7, 8675−8685

(36) Liakos, D. G.; Sparta, M.; Kesharwani, M. K.; Martin, J. M.; Neese, F. Exploring the Accuracy Limits of Local Pair Natural Orbital Coupled-Cluster Theory. *J. Chem. Theory Comput.* **2015**, *11*, 1525−1539.
(37) Lee, T. J.; Taylor, P. R. A Diagnostic for Determining the Quality of Single-Reference Electron Correlation Methods. *Int. J. Quantum Chem.* **1989**, 199−207.
(38) Wang, Q.-D.; Sun, M.-M.; Liang, J.-H. High-level theoretical study of the hydrogen abstraction reaction $H_2S + O_2 = SH + HO_2$ and prediction of the rate constants. *Comput. Theor. Chem.* **2019**, *1155*, 61−66.
(39) Rienstra-Kiracofe, J. C.; Allen, W. D.; Schaefer, H. F. The $C_2H_5+O_2$ reaction mechanism: High-level ab initio characterizations. *J. Phys. Chem. A* **2000**, *104*, 9823−9840.
(40) Frisch, M.; Trucks, G.; Schlegel, H.; Scuseria, G.; Robb, M.; Cheeseman, J.; Scalmani, G.; Barone, V.; Mennucci, B.; Petersson, G.; et al. *Gaussian 09, Revision D.01*; Gaussian, Inc.: Wallingford, CT, 2013.
(41) Neese, F. The ORCA program system. *Wiley Interdiscip. Rev.: Comput. Mol. Sci.* **2012**, *2*, 73−78.
(42) Neese, F.; Wennmohs, F.; Becker, U.; Riplinger, C. The ORCA quantum chemistry program package. *J. Chem. Phys.* **2020**, *152*, 224108.
(43) Barker, J. R. Multiple-Well, multiple-path unimolecular reaction systems. I. MultiWell computer program suite. *Int. J. Chem. Kinet.* **2001**, *33*, 232−245.
(44) Barker, J. R. Energy transfer in master equation simulations: A new approach. *Int. J. Chem. Kinet.* **2009**, *41*, 748−763.
(45) Barker, J. R.; Nguyen, T. L.; Stanton, J. F.; Aieta, C.; Ceotto, M.; Gabas, F.; Kumar, T. J. D.; Li, C. G. L.; Lohr, L. L.; Maranzana, A.; Ortiz, N. F.; Preses, J. M.; Simmie, J. M.; Sonk, J. A.; Stimac, P. J. *MultiWell-<2017.1> Software Suite, 2017.1*; University of Michigan: Ann Arbor, Michigan, USA, 2017. http://clasp-research.engin.umich.edu/multiwell/.
(46) Johnston, H. S.; Heicklen, J. Tunnelling Corrections for Unsymmetrical Eckart Potential Energy Barriers. *J. Phys. Chem.* **1962**, *66*, 532−533.
(47) Greenwald, E. E.; North, S. W.; Georgievskii, Y.; Klippenstein, S. J. A two transition state model for radical-molecule reactions: A case study of the addition of OH to C_2H_4. *J. Phys. Chem. A* **2005**, *109*, 6031−6044.
(48) Wang, Q.-D.; Sun, M.-M.; Liang, J.-H. Reaction Mechanisms and Kinetics of the Hydrogen Abstraction Reactions of C_4-C_6 Alkenes with Hydroxyl Radical: A Theoretical Exploration. *Int. J. Mol. Sci.* **2019**, *20*, 1275.
(49) Wu, J. J.; Khaled, F.; Ning, H. B.; Ma, L. H.; Farooq, A.; Ren, W. Theoretical and Shock Tube Study of the Rate Constants for Hydrogen Abstraction Reactions of Ethyl Formate. *J. Phys. Chem. A* **2017**, *121*, 6304−6313.
(50) Goodwin, D. G.; Speth, R. L.; Moffat, H. K.; Weber, B. W. *Cantera: An Object-oriented Software Toolkit for Chemical Kinetics, Thermodynamics, and Transport Processes, Version 2.4.0*, 2018.
(51) Klippenstein, S. J.; Cavallotti, C., Chapter 2 - Ab initio kinetics for pyrolysis and combustion systems. In *Mathematical modelling of gas-phase complex reaction systems: pyrolysis and combustion*, 2019; pp 115−167.
(52) Wang, Q.-D.; Sun, Y.; Sun, M.-M.; Liang, J.-H. Chemical Kinetics of Hydrogen Atom Abstraction from Propargyl Sites by Hydrogen and Hydroxy Radicals. *Int. J. Mol. Sci.* **2019**, *20*, 3227.
(53) Wang, Q.-D.; Liu, Z.-W. Reaction Kinetics of Hydrogen Atom Abstraction from C_4-C_6 Alkenes by the Hydrogen Atom and Methyl Radical. *J. Phys. Chem. A* **2018**, *122*, 5202−5210.

https://doi.org/10.1021/acsomega.1c06683
ACS Omega 2022, 7, 8675−8685